

Article

Searching for the optimal fluorophore to label antimicrobial peptides

Can Zhao, Antonio Fernandez, Nicolaos Avlonitis, Greetje
Vande Velde, Mark Bradley, Nick D. Read, and Marc VendrellACS Comb. Sci., **Just Accepted Manuscript** • DOI: 10.1021/acscmbosci.6b00081 • Publication Date (Web): 10 Oct 2016Downloaded from <http://pubs.acs.org> on October 13, 2016

Just Accepted

“Just Accepted” manuscripts have been peer-reviewed and accepted for publication. They are posted online prior to technical editing, formatting for publication and author proofing. The American Chemical Society provides “Just Accepted” as a free service to the research community to expedite the dissemination of scientific material as soon as possible after acceptance. “Just Accepted” manuscripts appear in full in PDF format accompanied by an HTML abstract. “Just Accepted” manuscripts have been fully peer reviewed, but should not be considered the official version of record. They are accessible to all readers and citable by the Digital Object Identifier (DOI®). “Just Accepted” is an optional service offered to authors. Therefore, the “Just Accepted” Web site may not include all articles that will be published in the journal. After a manuscript is technically edited and formatted, it will be removed from the “Just Accepted” Web site and published as an ASAP article. Note that technical editing may introduce minor changes to the manuscript text and/or graphics which could affect content, and all legal disclaimers and ethical guidelines that apply to the journal pertain. ACS cannot be held responsible for errors or consequences arising from the use of information contained in these “Just Accepted” manuscripts.



Searching for the optimal fluorophore to label antimicrobial peptides

Can Zhao,¹ Antonio Fernandez,² Nicolaos Avlonitis,³ Greetje Vande Velde,⁴ Mark Bradley,³
Nick D. Read,^{1,*} Marc Vendrell^{2,*}

¹ Manchester Fungal Infection Group, Institute of Inflammation and Repair, University of Manchester. CTF Building, Grafton St., M13 9NT Manchester, United Kingdom.

² MRC Centre for Inflammation Research, The University of Edinburgh. 47 Little France Crescent, EH16 4TJ Edinburgh, United Kingdom.

³ EaStCHEM School of Chemistry, The University of Edinburgh. West Mains Road, Edinburgh EH9 3FJ, United Kingdom.

⁴ Biomedical MRI Unit/MoSAIC, Department of Imaging and Pathology, KU Leuven, Leuven, Belgium.

KEYWORDS: fluorescence, labeling, imaging, probes, fungi, infection.

Abstract

1
2
3
4
5
6 With the advent of antimicrobial resistance, there is an urgent need for new strategies to treat
7
8 infectious diseases. Antimicrobial peptides are considered as promising candidates, and therefore
9
10 there is a need to understand their mechanism of action in order to exploit their therapeutic
11
12 potential. To this end, fluorescent analogs are powerful tools to analyze their behavior and
13
14 subcellular localization in cells and in vivo. However, the conjugation of fluorophores to
15
16 antimicrobial peptides, especially in short sequences, can impair their biological activity, making
17
18 the selection of the fluorescent label an essential step in these studies. In the present work, we
19
20 have systematically modified a model antifungal hexapeptide with a collection of fluorophores
21
22 covering broad physicochemical and spectral properties. The resulting conjugates have been
23
24 examined in two different fungal species, in terms of their activity and intracellular localization.
25
26 The biological results confirm the influence of the different fluorescent moieties on the
27
28 subcellular localization of antimicrobial sequences, and provides an insight on the optimal
29
30 fluorophores to be used in the preparation of fluorescent peptides for different bioimaging
31
32 assays.
33
34
35
36
37
38
39
40
41
42
43
44
45
46
47
48
49
50
51
52
53
54
55
56
57
58
59
60

Introduction

In the past decades, fluorescent dyes have been broadly used as tags to visualize and study the roles of peptides in cells and in vivo.¹ For these studies, live cell imaging has become the technology of choice as it provides a direct readout of the localization of the peptides with high spatial and temporal resolution. In the context of antimicrobial peptides, several reports have described fluorescence labeling as an approach to study their mechanism of action²⁻⁴ as well as to develop imaging probes for the rapid identification of microbes at infection sites.⁵ In all cases, it is often assumed that fluorescently labeled peptides faithfully mimic the spatio-temporal dynamics of the native peptides, and fluorescent labels are typically chosen on the basis of excitation/emission wavelength, quantum yield, photobleaching, environmental sensitivity or chemical conjugation. Little attention has been paid to whether the fluorescent label might alter the physicochemical properties of the conjugate, and it is often unclear whether the fluorescent tag influences the uptake and localization of antimicrobial peptides inside living cells. In order to evaluate the impact that different fluorophores have in the biological properties of antimicrobial peptides and their application as imaging probes, we have synthesized a library of fluorescent conjugates based on the Peptide Antifungal 26 (PAF26).⁶ This rationally designed hexapeptide exhibits high potency against filamentous fungi (including human and crop pathogens), low toxicity against bacterial cells and negligible toxicity against mammalian cells. PAF26 is currently being used a model peptide for the characterization of the mode-of-action of small, cationic, cell penetrating antifungal peptides and for the design and development of synthetic antifungal peptides with improved properties for therapeutic uses.⁷

1
2
3 In the present work, we have conjugated 12 different fluorophores (either in-house or
4 commercially available) to the peptide sequence of PAF26 and compared their biological
5 activity, cellular uptake and intracellular localization using confocal live cell imaging. From
6 these studies, we have observed that the activity of the conjugates is practically unaffected by the
7 fluorescent labels whereas they accumulate in different intracellular regions depending on the
8 fluorophore attached to the sequence. This systematic study will aid chemists working on
9 peptide-based imaging agents in the selection of the fluorophores for different fluorescence-
10 based biological applications.
11
12
13
14
15
16
17
18
19
20
21
22

23 **Results and Discussion**

24 **Design and synthesis of a library of fluorescent antifungal peptides**

25
26
27 For many years, the synthesis of antimicrobial peptides has been adapted to combinatorial
28 chemistry. However, libraries of antimicrobial peptides have been mainly focused on the
29 optimization of the peptide sequences, either to enhance their antimicrobial activity, improve
30 their selectivity against specific strains or pathogens, or to reduce their cytotoxicity in
31 mammalian cells.⁸⁻¹⁰ Some antimicrobial peptides have been labeled with fluorophores in order
32 to visualize their localization in cells by confocal microscopy.^{4,11} More recently, the high
33 selectivity of antimicrobial sequences has been exploited to develop imaging contrast agents for
34 the rapid identification of infection sites.^{12,13} In most reports, only one fluorophore is employed
35 on the basis of its compatibility with the experimental procedures. However, conventional
36 fluorophores differ largely in their physicochemical features,^{14,15} and therefore it is reasonable to
37 expect that different fluorophores could induce variability in the activity and cellular localization
38 properties of peptide sequences. For instance, Baker et al. reported the influence of different
39
40
41
42
43
44
45
46
47
48
49
50
51
52
53
54
55
56
57
58
59
60

1
2
3 fluorescent labels in a combinatorial library of A₁R adenosine inhibitors, where significant
4 differences were observed in the binding properties of several fluorescently-labeled inhibitors.¹⁶
5
6
7
8 In the context of short antimicrobial peptides, there are no reports of any systematic evaluation of
9 their biological properties after conjugation to various fluorescent labels. Herein, we have
10 designed a library based on the antimicrobial peptide sequence PAF26, which was modified with
11 a total of 12 fluorophores covering the whole spectral range (from blue to near-infrared
12 emission) and diverse physicochemical properties (Chart 1). In addition to conventional
13 fluorophores (e.g. carboxyfluorescein, carboxyrhodamine, BODIPY, cyanine), we also included
14 small fluorophores (e.g. NBD, dansyl), compounds with environmentally-sensitive properties
15 (e.g. Nile Blue, malachite green, styryl), pH-sensitivity (e.g. naphthalimide) and esterase-
16 activatable fluorophores (e.g. fluorescein diacetate). Overall, these fluorophores constitute a
17 representative collection of the fluorescent labels that most chemists would employ for labeling
18 any defined peptide sequence.
19
20
21
22
23
24
25
26
27
28
29
30
31
32
33
34
35
36
37
38
39
40
41
42
43
44
45
46
47
48
49
50
51
52
53
54
55
56
57
58
59
60

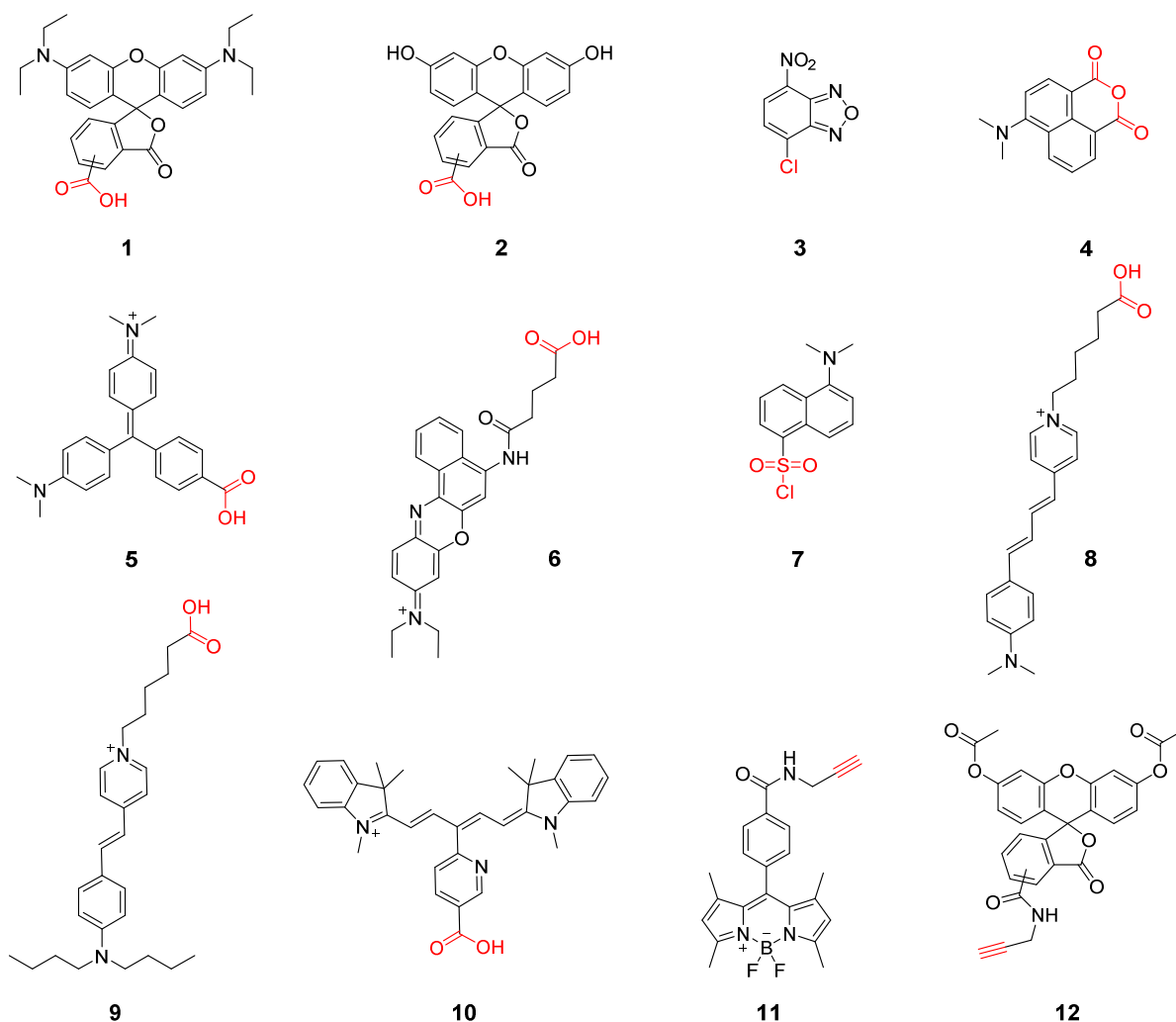
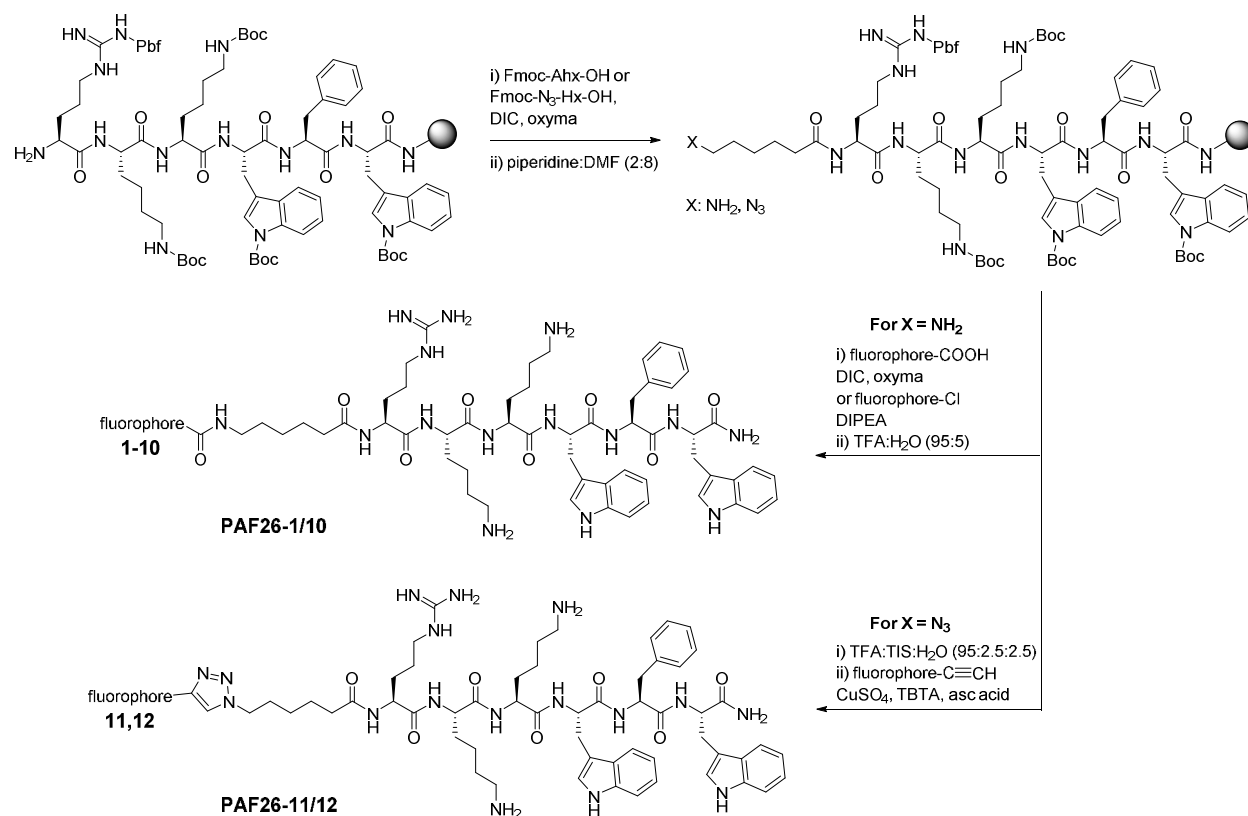


Chart 1. Fluorescent labels for the derivatization of the antimicrobial peptide PAF26. We employed 12 different fluorophores with suitable reactive groups (in red) for peptide labeling (e.g. carboxylic acids, sulfonyl chlorides, anhydrides, alkynes). Fluorophores **1**, **2**, **3** and **7** are commercially available, whereas the synthesis and characterization of all other fluorophores is described in the Experimental Procedures and the Electronic Supplementary Information (ESI).

PAF26 (H-RKKWFW-NH₂) is a short antimicrobial peptide which, like many other antimicrobial peptides, contains both cationic and hydrophobic residues,^{6,7} and therefore it is an excellent model for examining the influence of fluorophores in the properties of antimicrobial

1
2
3 peptides. We designed the synthesis of the hexapeptide using conventional solid-phase protocols
4
5 in Rink amide polystyrene resin (Scheme 1). In order to incorporate suitable conjugation groups
6
7 within the sequence of PAF26, we first synthesized two derivatives containing aminohexanoic or
8
9 azidohexanoic spacers directly attached to the *N*-terminal group of PAF26. Through these
10
11 spacers, fluorophores could be readily conjugated using their reactive groups (i.e., carboxylic
12
13 acids, chlorides, anhydrides, sulfonyl chlorides or alkynes) without affecting the main
14
15 recognition features of the antimicrobial peptide. Most library members were fully synthesized
16
17 on solid support, including the coupling of the fluorophore, to render the final fluorescent PAF26
18
19 analogues upon acidic cleavage from the resin using reported procedures.¹⁷ Due to the lability of
20
21 the fluorophores **11** and **12** (i.e., BODIPY and fluorescein diacetate, respectively) to acidic
22
23 media, the corresponding derivatives **PAF26-11** and **PAF26-12** were prepared by 1,3-Huisgen
24
25 dipolar cycloaddition using the azido-modified PAF26 and the fluorescent alkynes in solution
26
27 phase (Scheme 1). All 12 fluorescent derivatives of PAF26 were purified by semi-preparative
28
29 HPLC to isolate the final conjugates (**PAF26-1** to **PAF26-12**) in high purities (for
30
31 characterization data, see ESI).
32
33
34
35
36
37
38
39
40
41
42
43
44
45
46
47
48
49
50
51
52
53
54
55
56
57
58
59
60



31
32
33
34
35
36
37
38
39
40
41
42
43
44

Scheme 1. Solid-phase synthesis of a library of fluorescent antimicrobial peptides based on the hexapeptide PAF26. The peptide sequence of PAF26 was modified with amino- or azidohexanoic spacers at the *N*-terminus to enable the conjugation of different fluorophores, either by formation of amide bonds in solid-phase or by ‘click’ chemistry in solution. All 12 conjugates **PAF26-1** to **PAF26-12** were isolated in good yields and high purities. For the chemical structures of the fluorophores **1-12**, see Chart 1.

45 46 47 **In vitro biological activity of fluorescent antifungal peptides**

48
49
50
51
52
53
54
55
56
57
58
59
60

After completing the synthesis of the library of fluorescent antimicrobial conjugates (**PAF26-1** to **PAF26-12**), we measured their spectral properties and determined their IC₅₀ values in two different fungal species (i.e., *Neurospora crassa* and *Aspergillus fumigatus*) as a measure of their cellular activity (Table 1). *N. crassa* has been widely used as an experimental model organism for filamentous fungi.¹⁸ *A. fumigatus* is a very important opportunistic pathogen responsible for

1
2
3 multiple human diseases, the most lethal of which, invasive pulmonary aspergillosis, causes
4
5 around 200,000 deaths per year.¹⁹
6
7

8 Conjugates incorporating small fluorophores (e.g., NBD (**PAF26-3**), naphthalimide (**PAF26-4**),
9
10 dansyl (**PAF26-7**)) showed very similar antifungal activity when compared to the unlabeled
11
12 sequence PAF26 in both fungal species. This observation is in line with previous reports where
13
14 NBD or dansyl have been described as highly tolerated fluorescence labels for the derivatization
15
16 of biomolecules.²⁰ Larger fluorophores, including positively-charged fluorophores [i.e.
17
18 rhodamine (**PAF26-1**), Nile Blue (**PAF26-6**), styryl dyes (**PAF26-8** and **PAF26-9**)] and
19
20 fluorescein-based structures (**PAF26-2** and **PAF26-12**) induced only minor differences in the
21
22 antifungal activity of PAF26, with all IC₅₀ values in the low micromolar range. Two conjugates
23
24 (**PAF26-10** and **PAF26-11**) showed slightly higher activity, being the two corresponding
25
26 fluorophores [i.e. cyanine (**10**) and BODIPY (**11**)] permeable structures that have been reported
27
28 for the preparation of a range of fluorescent probes.²¹⁻²⁵ Altogether, these results corroborate the
29
30 minor influence of the fluorescence labels on the antifungal activity of fluorescent PAF26
31
32 conjugates, with the smallest impairment being observed for conjugates including small
33
34 fluorophores.
35
36
37
38
39
40
41
42
43
44
45
46
47
48
49
50
51
52
53
54
55
56
57
58
59
60

Table 1. Spectral properties and antifungal activities of the fluorescent antimicrobial sequences.

Compound	$\lambda_{\text{exc.}}$ (nm)	$\lambda_{\text{em.}}$ (nm)	MW	IC ₅₀ (<i>N. crassa</i> [‡])	IC ₅₀ (<i>A. fumigatus</i> [‡])
PAF26	n.d.	n.d.	949.6	4.0 ± 0.7	8.0 ± 0.3
PAF26-1 [‡]	563	593	1530.8	3.8 ± 0.1	6.9 ± 0.2
PAF26-2 [‡]	498	529	1419.7	5.3 ± 0.2	9.1 ± 0.3
PAF26-3	488	552	1225.6	4.4 ± 0.3	7.9 ± 0.1
PAF26-4	450	532	1285.7	4.2 ± 0.2	8.0 ± 0.2
PAF26-5	635	n.d.	1416.8	4.1 ± 0.4	9.7 ± 0.5
PAF26-6	635	679	1476.8	3.2 ± 0.2	5.8 ± 0.2
PAF26-7	300	350	1295.7	4.0 ± 0.1	7.9 ± 0.2
PAF26-8	465	706	1408.8	3.0 ± 0.1	7.7 ± 0.1
PAF26-9	487	621	1466.9	2.6 ± 0.2	7.2 ± 0.4
PAF26-10	633	660	1547.9	2.0 ± 0.1	4.2 ± 0.4
PAF26-11	505	540	1494.8	2.2 ± 0.2	3.7 ± 0.2
PAF26-12 [‡]	503	530	1585.7	5.3 ± 0.2	9.9 ± 0.4

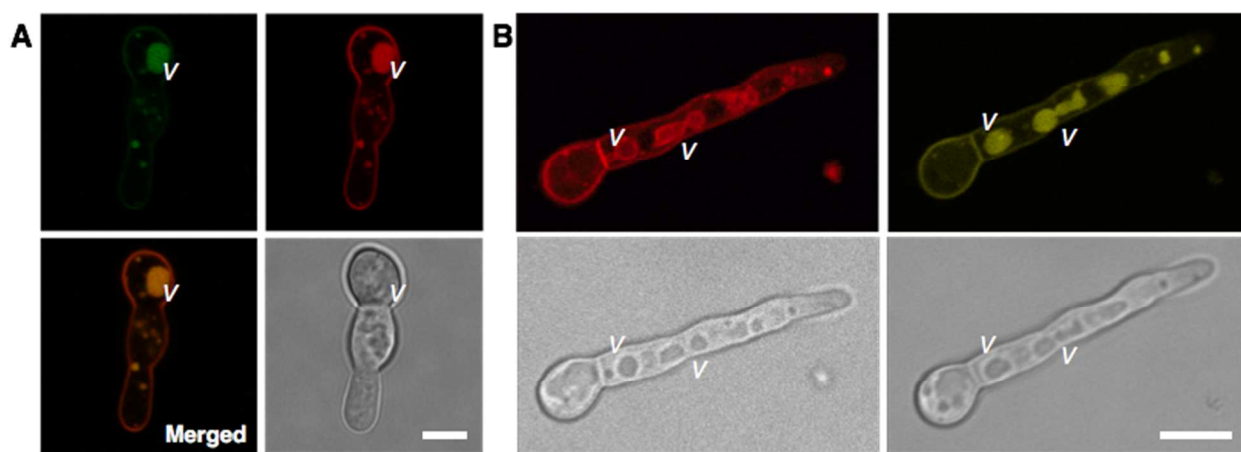
[‡] IC₅₀ values (μM) represented as means ± standard deviations (n=3).

[‡] Values obtained for the mixture of 5 and 6-carboxyisomers.

Fluorescence confocal live cell imaging studies to analyze the localization of PAF26 conjugates in fungal cells

Next we performed live cell imaging experiments to examine the cellular uptake and intracellular localization of the different conjugates in *N. crassa* and *A. fumigatus* by confocal laser scanning microscopy. Concentrations in the low micromolar range were used, as these have been previously optimized for the non-passive uptake of PAF26.¹⁶ As shown in Fig 1, the rhodamine PAF26-1 derivative localized to the cell envelope (comprising the plasma membrane and the cell wall) and the intracellular vacuolar/vesicular system of *N. crassa* conidial germlings, The

1
2
3 positive charge of the rhodamine fluorophore might favour the interaction with the negatively
4 charged phospholipids in the plasma membrane. In contrast, the carboxyfluorescein derivative
5
6 **PAF26-2** showed a similar pattern of intracellular vacuolar distribution but reduced staining on
7
8 the cell envelope (Fig. 1). The negative charge of carboxyfluorescein reduced the affinity of the
9
10 conjugate for the cell envelope, with slower internalization (Table 1). Similarly, the diacetylated
11
12 derivative (**PAF26-12**) showed preferential staining of the vacuolar lumens with no fluorescence
13
14 detected in the plasma or intracellular membranes, because its fluorescence emission is triggered
15
16 upon reaction with intracellular esterases (Fig. S1 in ESI). We performed co-localization
17
18 experiments between **PAF26-12** and **PAF26-1** and observed that both conjugates displayed a
19
20 similar pattern of cellular uptake, first appearing in small vesicles and then accumulating in
21
22 larger cell vacuoles (Fig. S2 in ESI).
23
24
25
26
27
28



45
46 **Figure 1. Confocal fluorescence microscope images of conidial germlings of *N. crassa* after**
47 **incubation with PAF26-1, PAF26-2 or PAF26-8.** A) Fluorescence images of *N. crassa* after
48 co-staining with the rhodamine **PAF26-1** derivative (red, 0.5 μ M) and the carboxyfluorescein
49 derivative **PAF26-2** (green, 0.5 μ M) at 25 $^{\circ}$ C. Scale bar: 2 μ m; v: vacuole. B) Imaging of *N.*
50 *crassa* after co-staining with the styryl **PAF26-8** derivative (red, 1 μ M) and the rhodamine
51 **PAF26-1** derivative (yellow, 1 μ M) at 25 $^{\circ}$ C. Scale bar: 5 μ m; v: vacuole.
52
53
54
55
56
57
58
59
60

1
2
3 Conjugates including small fluorophores, such as NBD (**PAF26-3**) or naphthalimide (**PAF26-4**),
4 displayed similar intracellular vacuolar/vesicular localization, both in conidial germlings of *N.*
5
6 *crassa* and *A. fumigatus* (Fig. S3 in ESI). Notably, the pH-sensitive properties of **PAF26-4**
7
8 enabled preferential imaging of acidified vacuoles as opposed to the general vacuolar and
9
10 vesicular structures staining observed with **PAF26-1** (Fig. S4 in ESI), demonstrating the
11
12 possibility of monitoring intracellular pH changes in these subcellular structures. Conjugates
13
14 including environmentally-sensitive fluorophores such as malachite green, Nile Blue or dansyl
15
16 (**PAF26-5**, **PAF26-6** and **PAF26-7**) showed marginal staining in fungal cells, suggesting the
17
18 potential accumulation of these peptide conjugates in neutral hydrophilic microenvironments
19
20 (e.g. vacuoles), in which these fluorophores exhibit very low quantum yields.^{26,27}
21
22
23
24
25
26
27

28 On the other hand, cationic styryl-based fluorophores (**PAF26-8** and **PAF26-9**) showed
29
30 remarkably enhanced staining of the envelope of fungal cells. **PAF26-8** brightly stained the
31
32 plasma and intracellular vacuolar/vesicular membranes of *N. crassa* to a similar extent than
33
34 **PAF26-1** (Fig. 1), but without marked accumulation in the vacuole lumens. Imaging experiments
35
36 using the **PAF26-9** derivative also showed a similar behavior in both *N. crassa* and *A. fumigatus*
37
38 (Fig. S5 in ESI). As observed for **PAF26-1**, the cationic character of the styryl fluorophores
39
40 favoured the rapid interaction with anionic components of the cellular membranes and enhanced
41
42 their internalization (Table 1). Interestingly, and in contrast to the results obtained with *N. crassa*
43
44 (Fig. 1), when we incubated **PAF26-8** with *A. fumigatus*, we did not observe the uptake of the
45
46 fluorescent conjugate into healthy cells and hyphae were only stained once the cell membrane
47
48 structure was compromised (Fig. S6 and Movie S1 in ESI). These results highlight differences in
49
50 the internalization of **PAF26-8** by cells of different fungal species, suggesting the possibility of
51
52 using fluorescent labels as means to improve the selectivity of antimicrobial sequences.
53
54
55
56
57
58
59
60

1
2
3 Finally, both cyanine and BODIPY-based conjugates (**PAF26-10** and **PAF26-11**, respectively)
4 displayed a markedly different staining pattern when compared to all other members of the
5 PAF26 library. The cyanine derivative (**PAF26-10**) brightly stained fungal cells and, besides
6 localizing within vacuoles and vesicle lumens, it also stained other cytoplasmic organelles. Dual
7 labeling experiments with the carboxyfluorescein derivative **PAF26-2** confirmed the presence of
8 **PAF26-10** in the same vacuolar and vesicular organelles but also indicated its localization in
9 different cytoplasmic organelles (Fig. 2). The BODIPY derivative **PAF26-11** exhibited general
10 staining of the cytoplasm with no specific accumulation in subcellular organelles, as shown by
11 co-localization experiments with **PAF26-1** (Fig. 2).
12
13
14
15
16
17
18
19
20
21
22
23
24

25 Furthermore, we compared the staining of *N. crassa* cells using the fluorescent peptides **PAF26-**
26 **1**, **PAF26-2**, **PAF26-10** and **PAF26-11** and their corresponding fluorophores alone (Fig S7 in
27 ESI). In these experiments, we observed that the PAF26 sequence is essential for the interaction,
28 internalization and accumulation of the fluorescent conjugates in the vacuoles of fungal cells, as
29 the fluorophores alone were not able to enter the cells or stained non-specifically intracellular
30 environments (e.g. the BODIPY fluorophore showed bright, general staining of lipid-rich
31 subcellular structures).
32
33
34
35
36
37
38
39
40
41
42
43
44
45
46
47
48
49
50
51
52
53
54
55
56
57
58
59
60

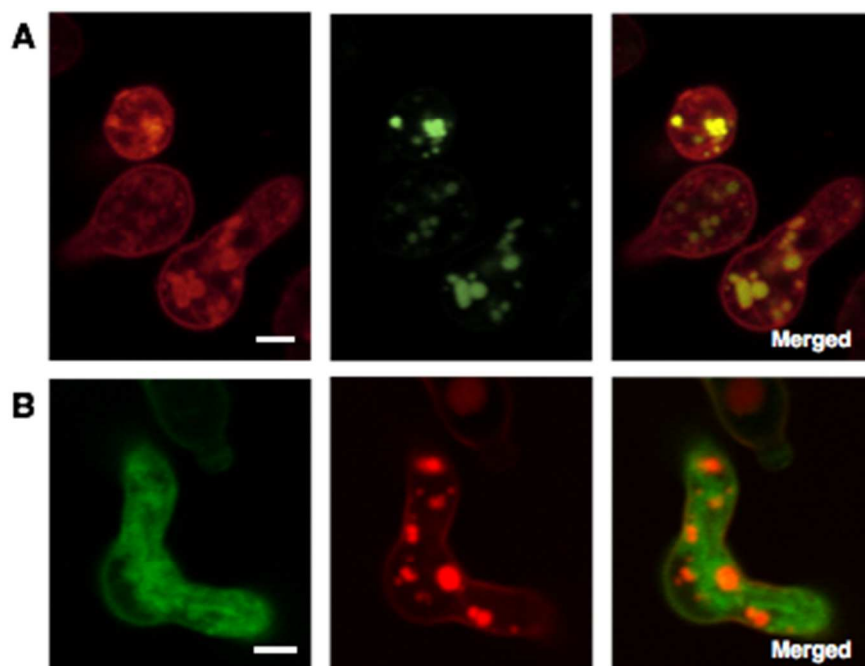


Figure 2. Fluorescence microscope images of conidial germlings of *A. fumigatus* after incubation with PAF26-10 or PAF26-11. A) Fluorescence images of *A. fumigatus* after co-staining with the cyanine **PAF26-10** (red, 1 μM) and the carboxyfluorescein **PAF26-2** (green, 1 μM) derivatives at 37 $^{\circ}\text{C}$. Scale bar: 1 μm . B) Fluorescence images of germinated *A. fumigatus* after co-staining with the BODIPY **PAF26-11** (green, 2 μM) and the rhodamine **PAF26-1** (red, 2 μM) derivatives at 37 $^{\circ}\text{C}$. Scale bar: 1 μm .

Finally, in view of the bright fluorescence signals in fungal cells upon incubation with **PAF26-10** (Figure 2A) and its emission in the near-infrared region ($\lambda_{\text{em.}}$: 660 nm, Table 1), we assessed the suitability of **PAF26-10** for whole-body in vivo fluorescence imaging experiments in mice with fungal lung infection. Near-infrared fluorophores are advantageous for in vivo imaging as the low autofluorescence background in such region of the spectra enhances the signal-to-noise ratios.²⁸⁻³⁰ We determined the background and fluorescence signals in mice that had been treated with **PAF26-10**, and observed that the cyanine fluorophore was bright enough to provide a

1
2
3 detectable signal from live animals using whole-body fluorescence imaging (Fig. S8 in ESI).
4
5 These results are in good agreement with previous reports of cyanine-labeled peptides for in vivo
6
7 imaging of cancer cells in xenograft models.^{31,32}
8
9

10
11 Altogether, the systematic evaluation of a library of fluorescent PAF26-based antimicrobial
12
13 peptides provided important clues of the optimal fluorophores for the preparation of fluorescent
14
15 peptides and their application in bioimaging experiments. Whereas positively-charged structures
16
17 (e.g. rhodamine, styryl) favor the interaction with the anionic membrane components, neutral
18
19 (e.g. NBD) and negatively-charged fluorophores (e.g. fluorescein) preferentially accumulate in
20
21 vacuoles, and pH-sensitive fluorophores (e.g. naphthalimide) offer the possibility of visualizing
22
23 specific intracellular processes in real time, such as vacuolar acidification. Cell permeable
24
25 fluorophores (e.g. cyanine) provide bright cytosolic staining and show good discrimination from
26
27 background signals in whole-body in vivo fluorescence imaging. These results suggest that,
28
29 whereas the PAF26 sequence is the main component responsible for the antifungal activity of the
30
31 fluorescent peptides, the incorporation of different fluorescent moieties into antimicrobial
32
33 sequences can lead to major redistributions of the peptide sequences to different subcellular
34
35 environments.
36
37
38
39
40
41
42

43 **Conclusions**

44
45
46 Fluorescently labeled peptides are powerful tools for image-based mechanistic studies in cells.
47
48 However, little is known about the influence of fluorescent tags in the uptake and localization of
49
50 peptides inside the cells, and fluorophores are primarily selected on the basis of their spectral
51
52 properties. We have evaluated the impact of different fluorophores (either commercially
53
54 available or synthetically accessible) in the biological properties of a small model antimicrobial
55
56
57
58
59
60

1
2
3 peptide by synthesizing a library of fluorescent derivatives of the antifungal hexapeptide PAF26.
4
5 Solid-phase peptide synthesis followed by conventional amide formation or solution-phase
6
7 ‘click’ conjugation for acid-sensitive fluorophores rendered a collection of 12 fluorescent
8
9 conjugates with broad spectral and physicochemical properties. The assessment of the
10
11 fluorescent peptides in two fungal species (*N. crassa* and *A. fumigatus*) indicated the minimal
12
13 impact of the fluorescent labels on the antimicrobial activity of the PAF26 sequence (with all
14
15 conjugates displaying IC₅₀ values in the low micromolar range) whereas major changes in the
16
17 localization pattern were observed upon conjugation to different fluorophores. This systematic
18
19 study will aid chemists working on peptide-based imaging agents in the selection of optimal
20
21 fluorophores for various fluorescence-based biological applications.
22
23
24
25
26
27
28
29
30
31
32
33
34
35
36
37
38
39
40
41
42
43
44
45
46
47
48
49
50
51
52
53
54
55
56
57
58
59
60

Experimental Procedures

8-(Dimethylamino)-3-oxatricyclo[trideca-1,5,7,9,11-pentaene]-2,4-dione (4). 2.0 mL of dimethylamine aqueous solution (19.9 mmol) and a catalytic amount of CuSO₄ were added to a suspension of 4-bromo-1,8-naphthalenedicarboxylic anhydride (1.9 mmol) in DMF (50 mL). The mixture was then refluxed for 1.5 h, after which the solvent was evaporated under vacuum. Compound **4** was crystallized from ethanol as a yellow solid (275 mg, 57% yield). HPLC: t_R = 4.74 min; MS (m/z): [M+H]⁺ calcd for C₁₄H₁₁NO₃: 242.1; found: 242.2; ¹H NMR (500 MHz, DMSO-*d*₆): δ 8.59 (d, *J* = 8.4 Hz, 1H), 8.46 (d, *J* = 7.2 Hz, 1H), 8.32 (d, *J* = 8.4 Hz, 1H), 7.76 (t, *J* = 7.9 Hz, 1H), 7.20 (d, *J* = 8.4 Hz, 1H), 2.51 (s, 6H); ¹³C NMR (126 MHz, DMSO-*d*₆): δ 162.0, 160.8, 157.8, 134.8, 133.6, 133.0, 125.5, 124.1, 119.3, 113.2, 108.4, 44.7.

***N*-(4-((4-carboxyphenyl)(4-(dimethylamino)phenyl)methylene)cyclohexa-2,5-dien-1-ylidene)-*N*-methylmethanaminium (5).** 4-(Bis(4-(dimethylamino)phenyl)methyl)benzoic acid (0.70 mmol) and *p*-chloranil (1.05 mmol) were dissolved in 30 mL CHCl₃, and 0.5 mL AcOH was added to the solution. The solution was stirred for 1.5 h at 35°C. Compound **5** was crystallized in water to yield a green solid (176 mg, 70% yield). HPLC: t_R = 4.28 min; MS (m/z): [M⁺] calcd for C₂₄H₂₅N₂O₂⁺: 373.2; found: 373.2; ¹H NMR (500 MHz, DMSO-*d*₆) δ 10.21 (s, 1H), 8.14 (d, *J* = 8.4 Hz, 2H), 7.46 (d, *J* = 8.4 Hz, 2H), 7.35 (d, *J* = 9.4 Hz, 2H), 7.11 (d, *J* = 9.5 Hz, 2H), 6.98 (d, *J* = 9.0 Hz, 2H), 6.64 (d, *J* = 9.0 Hz, 2H), 3.31 (s, 6H), 3.06 (s, 6H); ¹³C NMR (126 MHz, DMSO-*d*₆) δ 166.7, 157.0, 152.9, 151.6, 145.5, 144.6 (x 2), 140.5 (x 2), 132.7, 129.7, 128.9, 126.9 (x 2), 121.2 (x 2), 114.7 (x 2), 111.9 (x 2), 41.1 (x 2), 40.6 (x 2).

***N*-(5-(5-carboxybutanamido)-9*H*-benzo[*a*]phenoxazin-9-ylidene)-*N*-ethylethanaminium (6).** Nile Blue chloride (0.33 mmol) was dissolved in DCM together with glutaric anhydride (1 mmol) and DIPEA (1.14 mmol). The mixture was stirred at r.t. overnight. The crude mixture was then diluted with DCM and washed twice with water and then evaporated under vacuum. The

1
2
3
4
5
6
7
8
9
10
11
12
13
14
15
16
17
18
19
20
21
22
23
24
25
26
27
28
29
30
31
32
33
34
35
36
37
38
39
40
41
42
43
44
45
46
47
48
49
50
51
52
53
54
55
56
57
58
59
60

crude was then purified by column chromatography (DCM: MeOH, 9:1) to yield compound 6 as a dark blue solid (142 mg, 81% yield). HPLC: t_R : = 4.05 min; MS (m/z): $[M^+]$ calculated for $C_{25}H_{26}N_3O_4^+$: 432.2; found: 432.2; 1H NMR (500 MHz, DMSO- d_6) δ 8.75 (d, J = 8.0 Hz), 8.23 (s), 2.86 (q, J = 7.2 Hz), 2.35 (dt, J = 14.8 Hz, 4.6 Hz), 2.24 (t, J = 7.4 Hz), 1.93 – 1.77 (m), 1.71 (dd, J = 14.8 Hz, 7.4 Hz), 1.15 (d, J = 6.6 Hz); ^{13}C NMR (126 MHz, DMSO- d_6) δ 178.4, 174.6, 174.6, 164.2, 51.5, 33.3, 21.6, 21.3, 21.3, 20.5, 20.5, 19.1, 19.1, 18.9, 14.5, 14.5, 14.5, 12.3, 12.0.

1-(5-carboxypentyl)-4-((1E,3E)-4-(4-(Dimethylamino)phenyl)buta-1,3-dienyl)pyridin-1-ium

bromide (8). 4-Methylpyridine (5.4 mmol) and ethyl 6-bromohexanoate (6.5 mmol) were dissolved in 20 mL of ACN, the mixture was refluxed at 90°C overnight. 1-(6-ethoxy-6-oxohexyl)-4-methylpyridinium was precipitated in cold Et₂O:hexane (1:1) to yield a light brown solid (1.9 g, quantitative yield). HPLC: t_R : = 3.58 min; MS (m/z): $[M^+]$ calcd for $C_{14}H_{22}NO_2^+$: 236.2; found: 236.2. 1-(6-ethoxy-6-oxohexyl)-4-methylpyridinium (1.6 mmol) and 3-(4-(dimethylamino)phenyl)acrylaldehyde (2 mmol) were dissolved in 10 mL of EtOH in a microwave reaction vessel, then pyrrolidine (1.6 mmol) was added to the solution. The mixture was irradiated under microwave for 10 min at 120 °C, and the crude was purified by column chromatography (DCM: MeOH, 9:1) to yield 4-((1E,3E)-4-(4-(dimethylamino)phenyl)buta-1,3-dien-1-yl)-1-(6-ethoxy-6-oxohexyl)pyridin-1-ium bromide as a red solid (853 mg, quantitative yield). The ethyl ester (0.25 mmol) was dissolved in 2 mL THF and 1 mL MeOH, mixed with LiOH (1.25 mmol) in water (1 mL) and stirred overnight at r.t. to yield the carboxylic acid which was used *in situ* without any further purification. Characterization data for the ester: HPLC: t_R : = 4.73 min; MS (m/z): $[M^+]$ calcd for $C_{25}H_{33}N_2O_2^+$: 393.3; found: 393.4; 1H NMR (500 MHz, DMSO- d_6) δ 8.80 (d, J = 6.9 Hz, 2H), 8.05 (d, J = 7.0 Hz, 2H), 7.87 – 7.77 (m, 2H), 7.48 (d, J = 8.9 Hz, 2H), 7.02 (d, J = 6.6 Hz, 2H), 6.78 – 6.71 (m, 2H), 4.05 (q, J = 7.1 Hz, 2H), 2.99 (s, 6H),

1
2
3 2.31 (td, $J = 7.3, 2.1$ Hz, 2H), 1.95 – 1.83 (m, 2H), 1.61 – 1.52 (m, 2H), 1.38 – 1.25 (m, 2H),
4
5 1.19 (t, $J = 7.1$ Hz, 2H), 1.17 (t, $J = 7.1$ Hz, 3H). ^{13}C NMR (126 MHz, DMSO) δ 173.2, 153.6,
6
7 151.6, 144.1, 142.7, 129.6, 124.0, 123.6, 123.2, 112.5, 60.2, 59.5, 53.6, 33.6, 30.6, 25.3, 24.2,
8
9 23.0, 14.6.

10
11
12 **(*E*)-1-(5-carboxypentyl)-4-(4-(Dibutylamino)styryl)pyridin-1-ium bromide (9).** (*3E,5E*)- 1-
13
14 (6-ethoxy-6-oxohexyl)-4-methylpyridinium (1.6 mmol) and 4-(dibutylamino)benzaldehyde (2
15
16 mmol) were dissolved in 10 mL of EtOH in a microwave reaction vessel, then pyrrolidine (1.6
17
18 mmol) was added to the solution. The mixture was left to react under microwave irradiation for
19
20 10 min at 120°C. The crude was purified by column chromatography (DCM: MeOH, 9:1) to
21
22 yield (*E*)-4-(4-(dibutylamino)styryl)-1-(6-ethoxy-6-oxohexyl)pyridin-1-ium bromide as a purple
23
24 solid (703 mg, quantitative yield). The ethyl ester (0.25 mmol) was dissolved in 2 mL THF and 1
25
26 mL MeOH, mixed with LiOH (1.25 mmol) in water (1 mL) and stirred overnight at r.t. to yield
27
28 the carboxylic acid which was used *in situ* without any further purification. Characterization data
29
30 for the ester: HPLC: t_{R} : = 5.76 min; MS (m/z): [M^+] calcd for $\text{C}_{29}\text{H}_{43}\text{N}_2\text{O}_2^+$: 451.3; found: 451.4.
31
32 ^1H NMR (500 MHz, DMSO- d_6) δ 8.76 (d, $J = 7.0$ Hz, 2H), 8.05 (d, $J = 7.1$ Hz, 2H), 7.91 (d, $J =$
33
34 16.0 Hz, 1H), 7.57 (d, $J = 8.9$ Hz, 2H), 7.12 (d, $J = 16.0$ Hz, 1H), 6.74 (d, $J = 9.1$ Hz, 2H), 4.41
35
36 (t, $J = 7.4$ Hz, 2H), 4.05 (q, $J = 7.1$ Hz, 4H), 3.41 – 3.34 (m, 3H), 2.31 (td, $J = 7.3, 1.6$ Hz, 2H),
37
38 1.98 – 1.84 (m, 2H), 1.63 – 1.47 (m, 4H), 1.41 – 1.25 (m, 4H), 1.20 (t, $J = 7.1$ Hz, 3H), 1.17 (t, J
39
40 = 7.1 Hz, 3H), 0.93 (t, $J = 7.4$ Hz, 6H). ^{13}C NMR (126 MHz, DMSO) δ 173.2, 154.3, 150.4,
41
42 143.9, 142.8, 139.1, 131.0, 122.7, 122.2, 117.0, 112.0, 60.2, 59.3, 53.6, 50.3, 33.6, 30.6, 29.5,
43
44 25.3, 23.1, 20.1, 14.6.

45
46
47 **2-((1*E*,3*Z*)-3-(5-carboxypyridin-2-yl)-5-((*E*)-1,3,3-trimethylindolin-2-ylidene)penta-1,3-**
48
49 **dien-1-yl)-1,3,3-trimethyl-3*H*-indol-1-ium iodide (10).** 3*H*-Indolium-2,3,3-tetramethyl iodide
50
51
52
53
54
55
56
57
58
59
60

(0.72 mmol), NaOAc (0.72 mmol) and 6-(1,3-dioxopropan-2-yl) nicotinic acid (0.36 mmol) were added to a microwave reaction vessel with 10 mL Ac₂O:AcOH (1:1). The mixture was then heated up to 160°C under microwave irradiation for 0.5 h, after which the solvent was evaporated under vacuum. The crude was then purified using column chromatography (DCM:MeOH, 98:2 to 9:1) to yield compound **10** as a blue solid (144 mg, 80% yield). HPLC: t_R: = 4.72 min; MS (m/z): [M⁺] calcd for C₃₃H₃₄N₃O₂⁺: 504.3; found: 504.4; ¹H NMR (500 MHz, DMSO-*d*₆) δ 9.26 (d, *J* = 1.3 Hz, 1H), 8.44 (s, 1H), 8.41 (s, 1H), 8.40 (d, *J* = 2.2 Hz, 1H), 8.39 (d, *J* = 2.2 Hz, 1H), 7.65 (d, *J* = 7.4 Hz, 1H), 7.56 (d, *J* = 8.0 Hz, 1H), 7.42 (dd, *J* = 8.0, 1.2 Hz, 2H), 7.40 (d, *J* = 1.1 Hz, 3H), 7.28 (ddd, *J* = 7.4, 6.5, 1.9 Hz, 2H), 5.85 (d, *J* = 14.3 Hz, 1H), 3.39 (s, 6H), 1.76 (s, 12H). ¹³C NMR (126 MHz, DMSO) δ 177.5, 152.8, 152.4, 141.4, 139.9, 135.3, 133.7, 131.7, 131.1, 129.3, 128.8, 126.9, 126.3, 123.4, 11.9, 101.4, 52.6, 32.1, 27.5.

4-(1,3,5,5,7,9-Hexamethyl-5*H*-4λ⁴,5λ⁴-dipyrrolo[1,2-*c*:2',1'-*f*][1,3,2]diazaborinin-10-yl)-*N*-(prop-2-yn-1-yl)benzamide (11). 2,4-Dimethylpyrrole (4.5 mmol) and 4-carboxybenzaldehyde (2 mmol) were dissolved in DCM under Ar. One drop of TFA was added and the solution was stirred at r.t. until complete consumption of the aldehyde. Then, a solution of 2,3-dichloro-5,6-dicyano-1,4-benzoquinone (2 mmol) in DCM was added, and the stirring continued for 10 min followed by addition of triethylamine (4 mL) and BF₃Et₂O (4 mL). After stirring for another 2 h the reaction mixture was washed with water and dried, then solvent was evaporated under vacuum. The carboxylic acid was then purified by column chromatography (DCM: MeOH, 95:5). The crude product was then concentrated and precipitated (AcOEt: hexane, 1:1) to yield a dark red oil (160 mg, 20 % yield). HPLC: t_R: = 5.81 min; MS (m/z): [M⁺] calcd for C₂₀H₁₉BF₂N₂O₂: 368.2; found: 368.2. Then, the carboxylic acid (0.19 mmol) was dissolved with oxyma (0.57 mmol) in DCM and stirred for 5 min. DIC (1.14 mmol) was added and stirred for

1
2
3 another 2 min. Propargylamine (0.21 mmol) was then added and whole mixture was stirred at r.t.
4
5 for 3 h. Compound **11** was isolated as a bright orange solid (17 mg, 22% yield over all steps).
6
7 HPLC: t_R : = 5.80 min; MS (m/z): $[M+H]^+$ calcd for $C_{23}H_{22}BF_2N_3O$: 406.2; found: 406.2; 1H
8
9 NMR (500 MHz, DMSO- d_6) δ 8.05 (d, J = 8.4 Hz, 2H), 7.52 (d, J = 8.4 Hz, 2H), 6.20 (s, 2H),
10
11 5.76 (s, 1H), 4.09 (dd, J = 5.6, 2.5 Hz, 2H), 2.47 (s, 6H), 1.35 (s, 6H); ^{13}C NMR (126 MHz,
12
13 DMSO) δ 165.7, 143.2, 135.8, 134.8, 130.9, 128.7, 122.0, 112.1, 111.6, 98.8, 73.4, 29.1, 14.7,
14
15 14.6.
16
17
18
19

20 **3-Oxo-6-(prop-2-yn-1-ylcarbamoyl)-3H-spiro[isobenzofuran-1,9'-xanthene]-3',6'-diyl**

21 **diacetate (12).** 5,6-carboxyfluorescein diacetate (0.43 mmol) and oxyma (1.29 mmol) were
22
23 dissolved in DCM and stirred for 5 min. Then DIC (2.58 mmol) was added to the mixture, stirred
24
25 for 2 min and propargylamine (1.29 mmol) was added. The whole mixture was stirred at r.t. for 3
26
27 h then evaporated under vacuum. Compound **12** was purified by column chromatography (DCM:
28
29 MeOH: AcOH, 98:1:1) to yield a yellow oil (175 mg, 82% yield); HPLC: t_R : = 5.36 min; MS
30
31 (m/z): $[M+H]^+$ calcd for $C_{28}H_{19}NO_8$: 497.1; found: 497.8; 1H NMR (500 MHz, DMSO- d_6) δ 9.31
32
33 (t, J = 5.5 Hz, 1H), 9.13 (t, J = 5.5 Hz, 1H), 8.54 (dd, J = 1.6, 0.7 Hz, 1H), 8.29 (dd, J = 8.1, 1.6
34
35 Hz, 1H), 8.22 (d, J = 1.4 Hz, 1H), 8.16 (dd, J = 8.1, 0.7 Hz, 1H), 7.83 (t, J = 1.0 Hz, 1H), 7.55
36
37 (dd, J = 8.0, 0.7 Hz, 1H), 7.37 – 7.28 (m, 2H), 7.02 – 6.90 (m, 6H), 4.12 (dd, J = 5.5, 2.5 Hz,
38
39 2H), 4.00 (dd, J = 5.5, 2.5 Hz, 2H), 3.16 (t, J = 2.5 Hz, 1H), 3.08 (t, J = 2.5 Hz, 1H), 2.29 (s,
40
41 3H), 2.29 (s, 3H). ^{13}C NMR (126 MHz, DMSO) δ 170.3, 169.0, 167.4, 155.5, 152.4, 150.8,
42
43 135.5, 134.9, 130.0, 129.4, 119.1, 115.9, 110.6, 82.4, 81.4, 73.5, 29.6, 20.9.
44
45
46
47
48
49

50 **Solid-phase peptide synthesis.** All peptides were manually synthesized in polystyrene syringes
51
52 fitted with a polyethylene porous disc using Fmoc-based SPPS. Solvents and soluble reagents
53
54 were removed by suction. The Fmoc group was removed with piperidine: DMF (1:4) (1 \times 1 min,
55
56
57
58
59
60

1
2
3
4
5
6
7
8
9
10
11
12
13
14
15
16
17
18
19
20
21
22
23
24
25
26
27
28
29
30
31
32
33
34
35
36
37
38
39
40
41
42
43
44
45
46
47
48
49
50
51
52
53
54
55
56
57
58
59
60

2 × 10 min). Peptide synthesis transformations and washings were performed at r.t. For peptide elongation, after the Fmoc group was removed, resins were washed with DMF (4 × 1 min), DCM (3 × 1 min) and DMF (4 × 1 min). Unless otherwise noted, standard coupling procedures were used with DIC (3 eq.) and OxymaPure (3 eq.) in DMF for 1-2 h and 5-min of pre-activation. The completion of the coupling was monitored by the Kaiser test.³³ Then, resins were filtered and washed with DCM (4 × 1 min) and DMF (4 × 1 min).

Synthesis of the peptides PAF26-1/10. For conjugates **PAF26-1**, **PAF26-2**, **PAF26-5**, **PAF26-6**, **PAF26-8**, **PAF26-9**, **PAF26-10**, standard amide bond formation coupling conditions with fluorophore-COOH (3 eq.), DIC (3 eq.) and OxymaPure (3 eq.) in DMF were used. For compounds **PAF26-3**, **PAF26-4** and **PAF26-7**, coupling of the dyes was accomplished by incubation of the peptide with the fluorophore (3 eq.) and DIPEA (3 eq.) in DMF. All resins were then washed with DMF (4 × 1 min) and DCM (3 × 1 min). For the cleavages, resins were stirred in 5 mL of TFA: H₂O (95:5) for 2 h at r.t. as previously reported.³⁴ The beads were washed with TFA thoroughly and the peptides precipitated with ice-cold Et₂O after rotary evaporation before final purification by semi-preparative HPLC. Characterization details can be found in the ESI.

Synthesis of the peptides PAF26-11/12. Azido-derivatized peptides were cleaved from the resin by cleavage with 5 mL of TFA: H₂O: TIS (95:2.5:2.5) for 2 h at r.t. The beads were washed with TFA thoroughly and the peptides precipitated with ice-cold Et₂O after rotary evaporation. For the conjugation was performed, the peptide (1 eq.), ascorbic acid (1 eq.), tris[(1-benzyl-1*H*-1,2,3-triazol-4-yl)methyl] amine (TBTA) (0.3 eq.) and CuSO₄ (0.3 eq.) were dissolved in H₂O, and the corresponding alkynes (2 eq.) were added using a minimum amount of MeOH, leaving the reaction for approx. 4 h at r.t. The reaction was monitored with HPLC, and upon completion,

1
2
3 peptides were purified by semi-preparative HPLC. Characterization details can be found in the
4
5 ESI.
6
7

8 **Measurement of spectral properties.** Spectroscopic data were recorded on a Synergy HT
9
10 spectrophotometer (Biotek). Compounds were dissolved at concentrations around 10 μM -50 μM
11
12 in phosphate buffer saline (PBS) and spectra were recorded at r.t.
13
14

15 **Culturing of *N. crassa* and *A. fumigatus*.** Cultures of *N. crassa* (wild type strain # 2489 from
16
17 the Fungal Genetics Stock Center) and *A. fumigatus* (CEA10 strain from the fungal stock
18
19 collection of the Manchester Fungal Infection Group) were grown on solid 100% Vogel's agar
20
21 medium³⁵ at 25 °C for 3-5 days under constant light (*N. crassa*) or 37 °C for 4-5 days (*A.*
22
23 *fumigatus*). The spores (conidia) were then harvested from the plates with sterile deionized water
24
25 (*N. crassa*) or 0.05% Tween 80 in sterile deionized water (*A. fumigatus*), and the spore density
26
27 was determined with a haemocytometer.
28
29
30
31

32 **Antifungal activity measurements.** The BacTiter-GloTM Microbial Cell Viability Assay kit
33
34 (Promega), with CELLSTAR white polystyrene flat bottomed 96-well plates (Greiner), were
35
36 used for these assays. Each antifungal peptide, at an appropriate serial diluted concentrations,
37
38 was mixed with conidia of *N. crassa* or *A. fumigatus* to reach a final volume of 100 μL per well
39
40 and a final conidial concentration of 5×10^5 cells/mL in 10% liquid Vogel's medium. After 24 h
41
42 of incubation (at 25 °C for *N. crassa* or 37 °C for *A. fumigatus*), the amount of fungal growth was
43
44 determined by measurement of the luminescence in a TriStar LB 941 multimode microplate
45
46 reader. IC₅₀ values were determined using four parameter logistic regression. Data analysis was
47
48 performed using Sigma Plot 10.0. Values are represented as means \pm s.e.m. from two
49
50 independent experiments ($n = 3$).
51
52
53
54
55
56
57
58
59
60

1
2
3 **Confocal live cell microscopy.** Conidia at a concentration of 5×10^5 cells/mL were dispensed
4 into the wells of an 8-well slide culture chamber (ibidi USA Inc., Madison, WI) and incubated
5
6 for 3 h at 25 °C (*N. crassa*) or for 16 h at 37 °C (*A. fumigatus*) in 10% Vogel's medium in order
7
8 to allow germination to occur before the addition of antifungal peptide. The peptide was added to
9
10 produce the appropriate final concentration immediately before the live-cell imaging was
11
12 initiated. Individual germinated spores of each species were imaged for periods of up to 1 h at
13
14 the same temperature as they had previously been incubated at in a temperature-controlled
15
16 chamber mounted on the microscope stage. The live-cell imaging was performed with a Leica
17
18 TCS SP8 confocal laser scanning microscope equipped with photomultiplier tubes, hybrid
19
20 GaAsP detectors and a 63× water immersion objective and. White light (450-750 nm), argon ion
21
22 (458 nm, 476 nm, 488 nm and 496 nm) and blue diode lasers (405 nm) were used for excitation.
23
24 Images were processed and analyzed using Imaris 3D/4D image processing and analysis
25
26 software v 8.0 (Bitplane, Zurich, Switzerland). Details on the excitation and emission
27
28 wavelengths used for all of the **PAF26-1/12** conjugates are shown in Table S2 in the ESI.
29
30
31
32
33
34
35
36

37 **In vivo fluorescence imaging.** Animal experiments were carried out in compliance with national
38 and European regulations and were approved by the animal ethics committee of KU Leuven
39 (p103-2012). 9-week-old female Balb/C mice of (Balb/cAnNCrl from Charles River
40 Laboratories, bred at the KU Leuven animal facility, Leuven, Belgium) were kept in individually
41 ventilated cages with free access to food and water. Immune competent mice (n = 3) were
42 infected by inhalation of a fungal yeast cell suspension (*C. gattii* R265, 50,000 CFUs in 20 μL
43 PBS, 10 μL per nostril) under transient isoflurane gas anesthesia (2 % in pure O₂). Three weeks
44 after infection, whole-body fluorescence imaging was carried out under isoflurane anesthesia on
45
46 an IVIS Spectrum system with Living Image software (version 4.5.2, Perkin Elmer). The
47
48
49
50
51
52
53
54
55
56
57
58
59
60

1
2
3 fluorescence signal intensity was measured using the excitation/emission 640/680 filter pair
4
5 before and 5 min after intratracheal administration of 7.5 nmol of the **PAF26-10** derivative.
6
7

8
9 **Supporting Information.** NMR spectra and additional characterization data for the fluorescent
10
11 PAF26 conjugates, additional imaging data. This material is available free of charge via the
12
13 Internet at <http://pubs.acs.org>.
14
15

16 17 **Author Information**

18
19
20 The manuscript was written with contributions of all authors. All authors have given approval to
21
22 the final version of the manuscript.
23
24

25
26 * Corresponding authors: nick.read@manchester.ac.uk; marc.vendrell@ed.ac.uk
27
28

29 30 **Acknowledgements**

31
32 A.F. acknowledges funding from the Foundation Alfonso Martin Escudero (FAME, Spain).
33

34 G.V.V. acknowledges a postdoctoral fellowship of the Flemish Research Foundation (FWO).
35

36 N.D.R. acknowledges funding from the Scottish Universities Life Sciences Alliance (SULSA).
37

38
39 M.V. acknowledges funding from the Medical Research Council and the Marie Curie Career
40
41 Integration Grant (333487).
42
43

44 45 **Abbreviations**

46
47 PAF26, Peptide Antifungal 26; NBD-Cl, 4-chloro-7-nitro-2,1,3-benzoxadiazole; BODIPY, 4,4-
48
49 difluoro-4-bora-3a,4a-diaza-s-indacene; TFA, trifluoroacetic acid; DIC,
50
51 diisopropylcarbodiimide; DCM, dichloromethane, TBTA, tris(benzyltriazolylmethyl)amine.
52
53
54
55
56
57
58
59
60

References

- [1] González-Vera, J.A. Probing the kinome in real time with fluorescent peptides. *Chem. Soc. Rev.* **2012**, *41*, 1652-1664.
- [2] Mania, D.; Hilpert, K.; Ruden, S.; Fischer, R.; Takeshita, N. Screening for antifungal peptides and their modes of action in *Aspergillus nidulans*. *Appl. Environ. Microbiol.* **2010**, *76*, 7102-7108.
- [3] Maurya, I.K.; Pathak, S.; Sharma, M.; Sanwal, H.; Chaudhary, P.; Tupe, S.; Deshpande, M.; Chauhan, V.S.; Prasad, R. Antifungal activity of novel synthetic peptides by accumulation of reactive oxygen species and disruption of cell wall against *Candida albicans*. *Peptides* **2011**, *32*, 1732-1740.
- [4] Muñoz, A.; Marcos, J.F.; Read, N.D. Concentration-dependent mechanisms of cell penetration and killing by the *de novo*-designed antifungal hexapeptide PAF26. *Mol. Microbiol.* **2012**, *8*, 89-106.
- [5] Mendive-Tapia, L.; Zhao, C.; Akram, A.R.; Preciado, S.; Albericio, F.; Lee, M.; Serrels, A.; Kielland, N.; Read, N.D.; Lavilla, R.; Vendrell, M. Spacer-free BODIPY fluorogens in antimicrobial peptides for direct imaging of fungal infection in human tissue. *Nat. Commun.* **2016**, *7*, 10940 (DOI: 10.1038/ncomms10940).
- [6] Lopez-Garcia, B.; Perez-Paya, E.; Marcos, J. F. Identification of novel hexapeptides bioactive against phytopathogenic fungi through screening of a synthetic peptide combinatorial library. *Appl. Environ. Microbiol.* **2002**, *68*, 2453-2460.

1
2
3 [7] Muñoz, A.; Gandía, M.; Harries, E.; Carmona, L.; Read, N.D.; Marcos, J.F. Understanding
4 the mechanism of action of cell penetrating antifungal peptides using the rationally designed
5 hexapeptide PAF26 as a model. *Fungal Biol. Rev.* **2013**, *26*, 146-155.
6
7

8
9
10
11 [8] Sudheendra, U.S.; Dhople, V.; Datta, A.; Kar, R.K.; Shelburne, C.E.; Bhunia, A.;
12 Ramamoorthy, A. Membrane disruptive antimicrobial activities of human b-defensin-3 analogs.
13 *Eur. J. Med. Chem.* **2015**, *91*, 91-99.
14
15

16
17
18
19 [9] Torcato, I.M.; Huan, Y.H.; Franquelim, H.G.; Gaspar, D.; Craik, D.J.; Castanho, M.A.;
20 Troeira Henriques, S. Design and characterization of novel antimicrobial peptides, R-BP100 and
21 RW-BP100, with activity against Gram-negative and Gram-positive bacteria. *Biochim. Biophys.*
22 *Acta* **2013**, *1828*, 944-955.
23
24
25

26
27
28
29 [10] Gee, M.L.; Burton, M.; Grevis-James, A.; Hossain, M.A.; McArthur, S.; Palombo, E.A.;
30 Wade, J.D.; Clayton, A.H. Imaging the action of antimicrobial peptides on living bacterial cells.
31 *Sci. Rep.* **2013**, *3*, 1557.
32
33
34

35
36
37 [11] Scheinflug, K.; Krylova, O.; Nikolenko, H.; Thurm, C.; Dathe, M. Evidence for a novel
38 mechanism of antimicrobial action of a cyclic R-, W-rich hexapeptide. *PLoS One* **2015**, *10*,
39 e0125056.
40
41
42

43
44
45 [12] Welling, M.M.; Bunschoten, A.; Kuil, J.; Nelissen, R.G.H.H.; Beekman, F.J.; Buckle, T.;
46 van Leeuwen, F.W.B. Development of a hybrid tracer for SPECT and optical imaging of
47 bacterial infections. *Bioconjugate Chem.* **2015**, *26*, 839-849.
48
49
50

51
52
53 [13] Akram, A.R.; Avlonitis, N.; Lilienkamp, A.; Perez-Lopez, A.M.; McDonald, N.;
54 Chankeshwara, S.V.; Scholefield, E.; Haslett, C.; Bradley, M.; Dhaliwal, K. A labelled-
55
56
57
58
59
60

1
2
3
4
5
6
7
8
9
10
11
12
13
14
15
16
17
18
19
20
21
22
23
24
25
26
27
28
29
30
31
32
33
34
35
36
37
38
39
40
41
42
43
44
45
46
47
48
49
50
51
52
53
54
55
56
57
58
59
60

ubiquicidin antimicrobial peptide for immediate in situ optical detection of live bacteria in human alveolar lung tissue. *Chem. Sci.* **2015**, *6*, 6971–6979.

[14] Stockert, J.C.; Abasolo, M.I.; Blazquez-Castro, A.; Horobin, R.W.; Revilla, M.; Lombardo, D.M. Selective labelling of lipid droplets in aldehyde fixed cell monolayers by lipophilic fluorochromes. *Biotech. Histochem.* **2010**, *85*, 277-283.

[15] Lee, J.S.; Vendrell, M.; Chang, Y.T. Diversity-oriented optical imaging probe development. *Curr. Opin. Chem. Biol.* **2011**, *15*, 760-767.

[16] Baker, J.G.; Middleton, R.; Adams, L.; May, L.T.; Briddon, S.J.; Kellam, B.; Hill, S.J. Influence of fluorophore and linker composition on the pharmacology of fluorescent adenosine A1 ligands. *Br. J. Pharmacol.* **2010**, *159*, 772-786.

[17] Vendrell, M.; Angulo, E.; Casadó, V.; Lluís, C.; Franco, R.; Albericio, F.; Royo, M. Novel ergopeptides as dual ligands for adenosine and dopamine receptors. *J. Med. Chem.* **2007**, *50*, 3062-3069.

[18] Davis, R.H.; Perkins, D.D. Neurospora: a model of model microbes. *Nat. Rev. Genet.* **2002**, *3*, 397–403.

[19] Brown, G.D.; Denning, D.W.; Gow, N.A.; Levitz, S.M.; Netea, M.G.; White, T.C. Hidden killers: fungal human infections. *Sci. Transl. Med.* **2012**, *19*, 4, 165rv13.

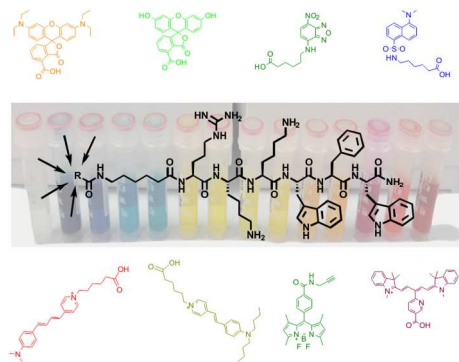
[20] Jansenn, M.J.; Ensing, K.; de Zeeuw, R.A. Fluorescent-labeled ligands for the benzodiazepine receptor. Part 2: The choice of an optimal fluorescent-labeled ligand for benzodiazepine receptor assays. *Pharmazie* **2000**, *55*, 102-106.

- 1
2
3 [21] Lee, J.S.; Kang, N.Y.; Kim, Y.K.; Kim, H.K.; Samanta, A.; Feng, S.; Vendrell, M.; Park,
4 J.H.; Chang, Y.T. Synthesis of a BODIPY library and its application to the development of live
5 cell glucagon imaging probe. *J. Am. Chem. Soc.* **2009**, *131*, 10077-10082.
6
7
8
9
10
11 [22] Samanta, A.; Vendrell, M.; Das, R.; Chang, Y.T. Development of photostable near-infrared
12 cyanine dyes. *Chem. Commun.* **2010**, *46*, 7406-7408.
13
14
15
16
17 [23] Zhai, D.; Lee, S.C.; Vendrell, M.; Leong, L.P.; Chang, Y.T. Synthesis of a novel BODIPY
18 library and its application in the discovery of a fructose sensor. *ACS Comb. Sci.* **2012**, *14*, 81-84.
19
20
21
22 [24] Er, J.C.; Vendrell, M.; Tang, M.K.; Zhai, D.; Chang, Y.T. Fluorescent dye cocktail for
23 multiplex drug-site mapping on human serum albumin. *ACS Comb. Sci.* **2013**, *15*, 452-457.
24
25
26
27
28 [25] Rimpelova, S.; Briza, T.; Kralova, J.; Zaruba, K.; Kejik, Z.; Cisarova, I.; Martasek, P.;
29 Ruml, T.; Kral, V. Rational design of chemical ligands for selective mitochondrial targeting.
30 *Bioconjugate Chem.* **2013**, *24*, 1445-1454.
31
32
33
34
35
36 [26] Tajalli, H.; Gilani, A.G.; Zaherhamidi, M.S.; Tajalli, P. The photophysical properties of Nile
37 red and Nile blue in ordered anisotropic media. *Dyes Pigments* **2008**, *78*, 15-24.
38
39
40
41 [27] Loving, G.S., Sainlos, M., Imperiali, B. Monitoring protein interactions and dynamics with
42 solvatochromic fluorophores. *Trends Biotechnol.* **2010**, *28*, 73-83.
43
44
45
46
47 [28] Frangioni, J.V. In vivo near-infrared fluorescence imaging. *Curr. Opin. Chem. Biol.* **2003**,
48 *7*, 626-634.
49
50
51
52 [29] Vendrell, M.; Samanta, A.; Yun, S.W.; Chang, Y.T. Synthesis and characterization of a cell-
53 permeable near-infrared fluorescent deoxyglucose analogue for cancer cell imaging. *Org.*
54 *Biomol. Chem.* **2011**, *9*, 4760-4762.
55
56
57
58
59
60

- 1
2
3 [30] Samanta, A., Vendrell, M., Yun, S.W., Guan, Z., Xu, Q.H., Chang, Y.T. A photostable near-
4 IR protein labeling dye for in vivo imaging. *Chem. Asian J.* **2011**, *6*, 1353-1357.
5
6
7
8
9 [31] Xin, J., Zhang, X., Liang, J., Xia, L., Yin, J., Nie, Y., Wu, K., Tian, J. In vivo gastric cancer
10 targeting and imaging using novel symmetric cyanine dye-conjugated GX1 peptide probes.
11 *Bioconjugate Chem.* **2013**, *24*, 1134-1143.
12
13
14
15
16
17 [32] Kim, E.M., Park, E.H., Cheong, S.J., Lee, C.M., Jeong, H.J., Kim, D.W., Lim, S.T., Sohn,
18 M.H. In vivo imaging of mesenchymal-epithelial transition factor (c-Met) expression using an
19 optical imaging system. *Bioconjugate Chem.* **2009**, *20*, 1299-1306.
20
21
22
23
24
25 [33] Kaiser, E., Colecott, R. L., Bossinger C. D., Cook, P. I. Color test for detection of free
26 terminal amino groups in the solid-phase synthesis of peptides. *Anal. Biochem.* **1970**, *34*, 595-
27 598.
28
29
30
31
32
33 [34] Yraola, F.; Ventura, R.; Vendrell, M.; Colombo, A.; Fernández, J. C.; de la Figuera, N.;
34 Fernández-Forner, D.; Royo, M.; Forns, P.; Albericio, F. A re-evaluation on the use of Rink,
35 BAL and PAL resins and linkers. *QSAR Comb. Sci.* **2004**, *23*, 145-152.
36
37
38
39
40
41 [35] Vogel, H. J. A convenient growth medium for Neurospora (Medium N). *Microbial Genet.*
42 *Bull.* **1956**, *13*, 42-43.
43
44
45
46
47
48
49
50
51
52
53
54
55
56
57
58
59
60

Table of Contents Graphic

Not just a pretty color. The synthesis and systematic evaluation of a library of fluorescent antimicrobial sequences provides new insights on the fluorophores of choice for different bioimaging applications.



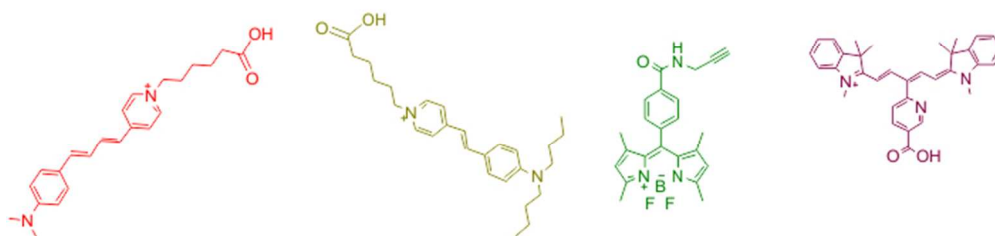
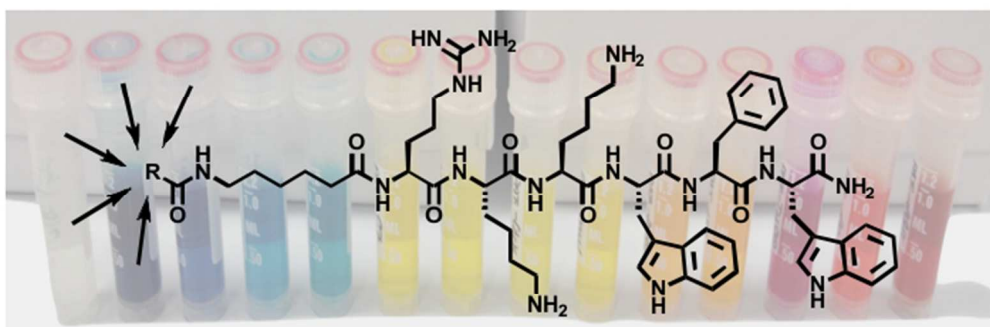
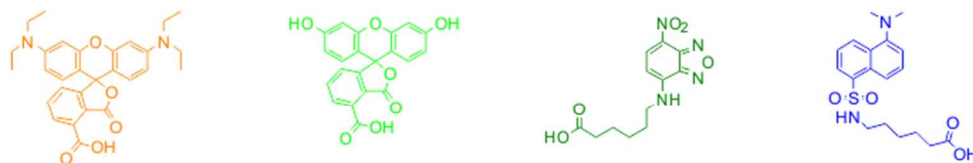


Table of Contents Graphic

59x46mm (300 x 300 DPI)